bioRxiv preprint doi: https://doi.org/10.1101/2021.02.02.428370; this version posted February 4, 2021. The copyright holder for this preprint (which was not certified by peer review) is the author/funder, who has granted bioRxiv a license to display the preprint in perpetuity. It is made available under aCC-BY-NC-ND 4.0 International license.

Full title: Protein lactylation induced by neural excitation

Short title: Protein lactylation in the brain

Authors: Hideo Hagihara[1], Hirotaka Shoji[1], Hikari Otabi[2,3], Atsushi Toyoda[2,3,4], Kaoru Katoh[5], Masakazu Namihira[5], Tsuyoshi Miyakawa[1*]

Affiliations:

[1] Division of Systems Medical Science, Institute for Comprehensive Medical Science, Fujita Health University, Aichi, Japan

[2] College of Agriculture, Ibaraki University, Ibaraki, Japan

[3] United Graduate School of Agricultural Science, Tokyo University of Agriculture and Technology, Tokyo, Japan

[4] Ibaraki University Cooperation between Agriculture and Medical Science (IUCAM), Ibaraki, Japan

[5]Biomedical Research Institute, National Institute of Advanced Industrial Science and Technology (AIST), Ibaraki, Japan

bioRxiv preprint doi: https://doi.org/10.1101/2021.02.02.428370; this version posted February 4, 2021. The copyright holder for this preprint (which was not certified by peer review) is the author/funder, who has granted bioRxiv a license to display the preprint in perpetuity. It is made available under aCC-BY-NC-ND 4.0 International license.

15 *Corresponding Author: Tsuyoshi Miyakawa (miyakawa@fujita-hu.ac.jp)

16 **Keywords:** lactylation, lactate, brain, posttranslational modification, histone H1

17

18 ORCID ID

19 Hideo Hagihara: https://orcid.org/0000-0001-9602-9518

20 Hirotaka Shoji: https://orcid.org/0000-0003-4843-6949

21 Hikari Otabi: https://orcid.org/0000-0001-5127-8190

22 Atsushi Toyoda: https://orcid.org/0000-0002-0245-3244

23 Kaoru Katoh: https://orcid.org/0000-0001-6590-413X

24 Masakazu Namihira: https://orcid.org/0000-0003-2108-5712

25 Tsuyoshi Miyakawa: https://orcid.org/0000-0003-0137-8200

bioRxiv preprint doi: https://doi.org/10.1101/2021.02.02.428370; this version posted February 4, 2021. The copyright holder for this preprint (which was not certified by peer review) is the author/funder, who has granted bioRxiv a license to display the preprint in perpetuity. It is made available under aCC-BY-NC-ND 4.0 International license.

Abstract

Lactate is known to have diverse roles in the brain at the molecular and behavioral levels under both physiological and pathophysiological conditions, such as learning and memory and regulation of mood. Recently, a novel post-translational modification called lysine lactylation has been found in histone H3 of mouse macrophages, and the lactylation levels paralleled the intracellular lactate levels[1]. However, it is unknown whether lysine lactylation occurs in brain cells, and if it does, whether lactylation is induced by the stimuli that accompany changes in lactate levels. Herein, we reveal that lysine lactylation in brain cells is regulated by systemic changes in lactate levels, neural excitation, and behaviorally relevant stimuli. Lysine lactylation levels were increased by lactate treatment and by high-potassium-induced depolarization in cultured primary neurons; these increases were attenuated by pharmacological inhibition of monocarboxylate transporter 2 and lactate dehydrogenase, respectively, suggesting that both cell-autonomous and non-cell-autonomous neuronal mechanisms are involved in overall lysine lactylation. *In vivo*, electroconvulsive stimulation increased lysine lactylation levels in the prefrontal cortices of mice, and its levels were positively correlated with the expression levels of the neuronal activity marker c-Fos on an individual cell basis. In the social defeat stress model of depression in which brain lactate levels increase, lactylation levels were increased in the prefrontal cortices of the defeated mice, which was accompanied by increased c-Fos expression, decreased social behaviors, and increased anxiety-like behaviors, suggesting

bioRxiv preprint doi: https://doi.org/10.1101/2021.02.02.428370; this version posted February 4, 2021. The copyright holder for this preprint (which was not certified by peer review) is the author/funder, who has granted bioRxiv a license to display the preprint in perpetuity. It is made available under aCC-BY-NC-ND 4.0 International license.

that stress-induced neuronal excitation may induce lysine lactylation, thereby affecting mood-related behaviors. Further, we identified 63 candidate lysine-lactylated proteins in the mouse cortex and found that lactylation levels in histone H1 increased in response to defeat stress. This study may open up an avenue for exploration of a novel role of neuronal activity-induced lactate mediated by protein lactylation in the brain.

bioRxiv preprint doi: https://doi.org/10.1101/2021.02.02.428370; this version posted February 4, 2021. The copyright holder for this preprint (which was not certified by peer review) is the author/funder, who has granted bioRxiv a license to display the preprint in perpetuity. It is made available under aCC-BY-NC-ND 4.0 International license.

Main text

Lactate in the brain has emerged as an energy substrate and a valuable signaling molecule[2], and its alteration has been implicated in multiple neuropsychiatric disorders. Among various strains/conditions of animal models of neuropsychiatric disorders, we have identified more than 20 out of 65 strains/conditions of mice that show altered lactate levels in whole brain[3,4]. A recent research identified lysine lactylation (Kla) as a novel post-translational modification in histone protein that can be stimulated by lactate[1]. A report by Zhang et al. suggested that histone H3 Kla mediates a metabolic alteration-related lactate regulation of gene expression in mouse bone marrow-derived macrophages[1]. The following reports have described key roles of lactate-induced Kla in macrophages in the transition of macrophages from a proinflammatory state to a reparative state[5] and the pathogenesis of lung fibrosis[6]. However, it has not been elucidated whether this Kla occurs and is regulated by exogenous lactate treatment or by stimulation that increases endogenous lactate levels in other types of cells/tissues including brain cells.

bioRxiv preprint doi: https://doi.org/10.1101/2021.02.02.428370; this version posted February 4, 2021. The copyright holder for this preprint (which was not certified by peer review) is the author/funder, who has granted bioRxiv a license to display the preprint in perpetuity. It is made available under aCC-BY-NC-ND 4.0 International license.

Lactate treatment and neuronal excitation increase protein lactylation in the brain

Kla was detected by western blot analysis in mouse brain tissues, with patterns different from those observed in macrophages and peripheral organs (Fig. 1a, Extended Data Fig. 1). With confocal microscopic imaging, we observed Kla signals throughout the cell, including somata and neurites, with a relatively weak signal in the nucleus region in primary cultured neurons expressing the neuronal marker βIII-tubulin (Fig. 1b). These results suggest that Kla modifications occur in various proteins to varying degrees, potentially with neural cell-specific functional roles different from those found in macrophages.

We investigated whether extracellular application of lactate stimulates Kla in neuronal cells as seen in macrophages[1]. Lactate treatment significantly increased Kla immunoreactivity in the primary cultured neurons (Fig. 1c, d), as confirmed by an independent experiment performed at a different institute (Extended Data Fig. 2). The increase in Kla immunoreactivity was attenuated in a dose-dependent manner by α-cyano-4-hydroxycinnamate (4-CIN), a monocarboxylate transporter 2 (MCT2) inhibitor that blocks lactate transport into neurons (Fig. 1d). Considering that there are few astrocyte-like cells

bioRxiv preprint doi: https://doi.org/10.1101/2021.02.02.428370; this version posted February 4, 2021. The copyright holder for this preprint (which was not certified by peer review) is the author/funder, who has granted bioRxiv a license to display the preprint in perpetuity. It is made available under aCC-BY-NC-ND 4.0 International license.

in the culture (Fig. 1e), lactate derived from astrocytes may minimally affect the lactate contents therein. Furthermore, in an *in vivo* experiment, we found that chronic and systemic treatment with lactate, shown to increase extracellular lactate concentrations in the brain[7], increased Kla immunoreactivity in the mouse prefrontal cortex (PFC) (Fig. 1f–h), but not in the hippocampus (Extended Data Fig. 3), suggesting that exogenous lactate stimulates protein lactylation in the brain in a region-dependent manner.

To examine in what neural cell types protein lactylation occurs in the brain, we conducted double-immunostaining of Kla with cell type-specific markers on mouse PFC: Camk2a for glutamatergic neurons, GAD67 for GABAergic neurons, S100b for astrocytes, and CD68 for microglia. Kla immunoreactivity was found in all cell types examined, suggesting that protein lactylation may ubiquitously occur in neural cells in the brain (Fig. 1i).

Neuronal excitation stimulates protein lactylation in the brain

bioRxiv preprint doi: https://doi.org/10.1101/2021.02.02.428370; this version posted February 4, 2021. The copyright holder for this preprint (which was not certified by peer review) is the author/funder, who has granted bioRxiv a license to display the preprint in perpetuity. It is made available under aCC-BY-NC-ND 4.0 International license.

Neuronal excitation increases brain lactate levels[8–12]. We examined lactate and protein lactylation levels using an *in vitro* neuronal excitation model. Primary neuron cultures were treated with a high concentration of potassium ions (high-K) (Fig. 2a) to induce depolarization of neurons *in vitro*. The high-K treatment resulted in increased lactate concentration in the culture supernatant at 30 minutes after the initiation of treatment (Fig. 2b). The intracellular lactate level showed a trend of time-dependent increase and reached significant increase at 2 hours after the initiation of high-K treatment (Fig. 2b). The high-K-induced increase in Kla levels was attenuated by treatment with sodium oxamate (OX), which inhibits lactate dehydrogenase (LDH) activity in neural[13,14] and other cell types [1] (Fig. 2c), suggesting that neuronal excitation may induce protein lactylation via intracellular metabolism and the glycolytic pathway. To test this hypothesis *in vivo*, we treated mice with electroconvulsive stimulation (ECS) and then examined lactate and protein lactylation levels in the brain. The brain lactate levels increased 10 minutes after ECS and persisted for 1 hour (Fig. 2d, e). We then examined Kla levels in mouse brains treated with ECS in combination with OX and/or 4-CIN (Fig. 2f). While the ECS-induced increase in Kla immunoreactivity was

bioRxiv preprint doi: https://doi.org/10.1101/2021.02.02.428370; this version posted February 4, 2021. The copyright holder for this preprint (which was not certified by peer review) is the author/funder, who has granted bioRxiv a license to display the preprint in perpetuity. It is made available under aCC-BY-NC-ND 4.0 International license.

not significantly affected by prior treatment with either OX or 4-CIN alone, it was attenuated by a combination treatment with OX and 4-CIN (Fig. 2g, h), suggesting that, *in vivo*, both intracellular new lactate production and extracellular lactate uptake have a role in neuronal activation-induced protein lactylation in the acute phase.

c-Fos is an immediate early gene product used as a marker for neuronal activation[15]. Utilizing the characteristics of c-Fos expression, we investigated the relation between Kla and c-Fos expressions in the ECS mouse model. Upon double-immunostaining analysis of c-Fos-expressing cells in the PFC, we found a significant positive correlation between Kla and c-Fos immunoreactive intensities on an individual cell basis level (Fig. 2i, j, Extended Data Fig. 4). Considering that intensity of electrical stimulation positively correlates with c-Fos-labeling levels in individual neurons[16], our results suggest that the more neurons are activated, the more Kla is induced in the cells. However, we have to note that there also are many cells that are Kla-positive but c-Fos-negative, suggesting that some Kla formations are independent of neuronal activation or lasts longer than that of c-Fos protein expression after neuronal activation.

bioRxiv preprint doi: https://doi.org/10.1101/2021.02.02.428370; this version posted February 4, 2021. The copyright holder for this preprint (which was not certified by peer review) is the author/funder, who has granted bioRxiv a license to display the preprint in perpetuity. It is made available under aCC-BY-NC-ND 4.0 International license.

Social stress stimulates protein lactylation in the brain

We explored whether protein lactylation in the brain is modified by a physiologically relevant stimulus using a social defeat stress (SDS) model of depression. SDS has been shown to increase c-Fos expression levels in many brain regions[17–19]. Brain lactate levels increased immediately (10 minutes) after a single exposure to the stress, and the increase was attenuated by prior treatment with OX[1] (Extended Data Fig. 5).

Further, we conducted a chronic experiment where the mice experienced daily defeat stress with prior treatment with OX or vehicle (saline) for 10 consecutive days. To examine the correlation between brain lactate and Kla levels and behavioral measures of anxiety and depression, we conducted a series of behavioral tests prior to brain sampling (Fig. 3a, Extended Data Fig. 6, 7). In the social avoidance test, the social interaction ratio decreased in both chronic vehicle-treated and OX-treated socially defeated mice compared to control mice (Fig. 3b). Based on the standard criteria[20,21], we focused on mice susceptible

bioRxiv preprint doi: https://doi.org/10.1101/2021.02.02.428370; this version posted February 4, 2021. The copyright holder for this preprint (which was not certified by peer review) is the author/funder, who has granted bioRxiv a license to display the preprint in perpetuity. It is made available under aCC-BY-NC-ND 4.0 International license.

139 to SDS, which showed a social interaction ratio <1 in the social avoidance test and
140 designated them as defeated mice for the following behavioral and brain tissue analyses.

141 We found that brain lactate levels were higher in defeated mice than in control
142 mice (Fig. 3c), as confirmed by independent sets of mice (Extended Data Fig. 8). Brain lactate
143 levels were paradoxically increased in OX-treated defeated mice at 9 days after the last
144 stress exposure and OX treatment compared to vehicle-treated defeated mice and control
145 mice (Fig. 3c). Simple correlation (Fig. 3d; Extended Data Fig. 9) and multiple regression
146 (Extended Data Table 1) analyses suggested that increased brain lactate levels are
147 preferentially associated with increased anxiety-like behaviors. In this stress model, Kla
148 levels in the PFC were increased in vehicle-treated defeated mice and, to a larger extent, in
149 OX-treated defeated mice compared to control mice (Fig. 3e, f).

150 Expression of neuronal activity marker c-Fos in the PFC also increased in vehicle-
151 treated defeated mice and, to a lager extent, in OX-treated defeated mice, in both a familiar
152 environment in the home cage (non-stimulated basal condition) and novel environment
153 exposed to the open field (condition with anxiogenic stimulation) (Fig. 3g, h). In the mice

bioRxiv preprint doi: https://doi.org/10.1101/2021.02.02.428370; this version posted February 4, 2021. The copyright holder for this preprint (which was not certified by peer review) is the author/funder, who has granted bioRxiv a license to display the preprint in perpetuity. It is made available under aCC-BY-NC-ND 4.0 International license.

that received anxiogenic stimulation to ensure more c-Fos-expressing cells, we found that the Kla level positively correlated with the c-Fos expression level in the PFC (Fig. 3i). Although changes in Kla and c-Fos expression levels were observed in some other brain regions implicated in anxiety and depression behaviors (e.g., hippocampus, lateral habenula, and amygdala; Extended Data Fig. 10, 11), no significant correlations were found between Kla and c-Fos expression levels in brain regions other than the PFC (Extended Data Fig. 12), suggesting that simultaneous induction of c-Fos and Kla occurs in a brain region-specific manner following repeated SDS. Furthermore, we found that Kla levels in the PFC, but not in the amygdala and hippocampal subregions, negatively correlated with the social interaction ratio in the social avoidance test (Fig. 3j, Extended Data Fig. 13) and with distance traveled in the dark compartment in the light–dark transition test (Fig. 3k), indicating that the more susceptible to SDS and the more anxious the mouse is, the higher the Kla levels in the PFC.

Identification of lactylated proteins in the brain

bioRxiv preprint doi: https://doi.org/10.1101/2021.02.02.428370; this version posted February 4, 2021. The copyright holder for this preprint (which was not certified by peer review) is the author/funder, who has granted bioRxiv a license to display the preprint in perpetuity. It is made available under aCC-BY-NC-ND 4.0 International license.

We sought to identify and quantify the brain proteins modified by lactylation and whose lactylation levels changed in response to SDS. Accordingly, we analyzed the PFC of defeated and control mice using Kla antibody immunoprecipitation and mass spectrometry techniques. This analysis identified 63 candidate lysine-lactylated proteins in the mouse PFC (Extended Data Table 2). GO-enrichment analysis with DAVID[22,23] showed that these proteins were mainly enriched in nucleosome- and histone-related biological processes (Extended Data Table 3). Among them, 12 proteins were suggested to be changed by SDS, of which seven were upregulated and five were downregulated. Notably, four subtypes of histone H1 were included in the 12 changed proteins and all were upregulated, suggesting that SDS increases lactylation at histone H1. We confirmed these observations by conducting immunoprecipitation with the histone H1 antibody followed by western blot analysis with the Kla antibody (Extended Data Fig. 14). In the PFC, 59.5% of cells were positive for histone H1 and nearly all the histone H1-positive cells (94.6%) were Kla positive, and vice versa (99.1% of Kla-positive cells were histone H1 positive) (Fig. 4a, b). Upon super-resolution imaging using stimulated emission depletion (STED) microscopy, we observed

bioRxiv preprint doi: https://doi.org/10.1101/2021.02.02.428370; this version posted February 4, 2021. The copyright holder for this preprint (which was not certified by peer review) is the author/funder, who has granted bioRxiv a license to display the preprint in perpetuity. It is made available under aCC-BY-NC-ND 4.0 International license.

184 histone H1 and Kla double-positive structures in the nucleus, suggestive of lysine lactylation
185 at histone H1 (Fig. 4c). Importantly, the double-positive structures in the nucleus increased
186 in the defeated mice compared to control mice (Fig. 4d), further supporting that SDS
187 enhances lysine lactylation levels at histone H1 in the PFC.

188

189 **Discussion**

190 In this study, we showed that a novel post-translational modification called lysine
191 lactylation occurs in brain cells and that its levels can be changed by neuronal excitation.
192 We found that increasing lactate levels by lactate addition or inducing neuronal excitation
193 with high-K or ECS increased Kla levels in the mouse brain cells both *in vitro* and *in vivo*. The
194 lactate and Kla levels also increased by behaviorally induced neuronal excitation associated
195 with SDS. In the SDS model of depression, Kla levels in the PFC, a core brain region
196 implicated in depressive and anxiety disorders, correlated with anxiety-like behaviors,
197 suggesting a potential behavioral significance of Kla in the brain. Furthermore, our

bioRxiv preprint doi: https://doi.org/10.1101/2021.02.02.428370; this version posted February 4, 2021. The copyright holder for this preprint (which was not certified by peer review) is the author/funder, who has granted bioRxiv a license to display the preprint in perpetuity. It is made available under aCC-BY-NC-ND 4.0 International license.

198 proteomic approach identified 63 candidate lactylated proteins in the mouse PFC and
199 highlighted that histone H1 lactylation increases in response to chronic stress.

200 Our results using SDS model mice suggest that, in stress-related pathological
201 conditions, excess neuronal activity may underlie increased protein lactylation in the PFC,
202 potentially associated with susceptibility to stress and anxiety-like behavior, although the
203 causal mechanism remained unclear. Given that increased Kla levels reflect neuronal
204 activity, it might be expected that significant correlations can be seen between Kla levels in
205 the brain regions other than PFC and behavioral alterations. Adaptation in neuronal activity
206 has been suggested to occur following repeated SDS in some brain regions; for example,
207 neurons in the central nucleus of amygdala became less active and showed suppressed c-
208 Fos expression after repeated SDS[24]. Such adaptation in neuronal activity may affect c-Fos
209 expression, possibly as well as Kla induction, resulting in no clear correlations between
210 behavior and Kla levels in brain regions other than the PFC.

211 Regarding the mechanisms of Kla formation, Zhang et al. showed that, using a ^{13}C-
212 labeled L-lactate incorporation method, Kla could be derived directly from lactate

bioRxiv preprint doi: https://doi.org/10.1101/2021.02.02.428370; this version posted February 4, 2021. The copyright holder for this preprint (which was not certified by peer review) is the author/funder, who has granted bioRxiv a license to display the preprint in perpetuity. It is made available under aCC-BY-NC-ND 4.0 International license.

213 exogenously applied to mouse bone marrow-derived macrophages[1]. Conversely, other
214 studies have suggested that Kla formation could be mediated indirectly by a glycolytic
215 intermediate, lactoylglutathione, which can provide a lactyl group to lysine residues. L-
216 Lactate is suggested to suppress the activity of glyoxalase 2, an enzyme catalyzing the
217 conversion of lactoylglutathione into glutathione and free D-lactate. Such suppression due
218 to increased L-lactate could elevate lactoylglutathione levels, which in turn, may facilitate
219 the indirect lactylation pathway. Gaffney et al. used a stable isotope labeling of amino acids
220 in cell culture (SILAC) model to identify lactylated proteins that could be formed via
221 lactoylglutathione in the HEK293 cell line[25]. The identified proteins were enriched in
222 glycolytic and carbon-metabolism enzymes but did not include histone family proteins. As
223 mentioned above, Kla forms directly from lactate on histone H3[1]. Our list includes histone
224 H3 as well as the 60S ribosomal protein L30 and Rho guanine nucleotide exchange factor 2,
225 also found in the 350-protein list published by Gaffney et al.[25] These observations suggest
226 that direct and indirect lactylation pathways may coexist, rather than being exclusive,

bioRxiv preprint doi: https://doi.org/10.1101/2021.02.02.428370; this version posted February 4, 2021. The copyright holder for this preprint (which was not certified by peer review) is the author/funder, who has granted bioRxiv a license to display the preprint in perpetuity. It is made available under aCC-BY-NC-ND 4.0 International license.

227 depending on the proteins expressed in the brain. Regardless of the mechanisms, lysine
228 lactylation may play a role in coupling metabolic changes to gene-expression regulation.

229 Our analyses highlighted that H1 histones increase their Kla levels in response to
230 SDS. Histone H1 is known to be a linker histone, having a key role in higher-order chromatin
231 folding and genome stability. Seven subtypes of H1 histone have been identified in
232 mammalian somatic cells, i.e., H1.0–1.5 and H1.10[26]. Numerous post-translational
233 modifications have been identified in H1, such as phosphorylation, methylation, acetylation,
234 formylation, crotonylation, and citrullination[27]. Post-translational modifications of histone
235 H1 have received less attention than those of core histones; therefore, knowledge on the
236 functional role of H1 modifications is limited[26,28], especially in brain cells. In the case of
237 mouse macrophage histone H3, lactylation competes with acetylation at lysine residues to
238 regulate the expression of a specific gene set. Extrapolating these findings to histone H1
239 and considering that histone H1 acetylation regulates chromatin compaction and
240 decondensation and hence the accessibility of linker DNA regions to transcription factors,

bioRxiv preprint doi: https://doi.org/10.1101/2021.02.02.428370; this version posted February 4, 2021. The copyright holder for this preprint (which was not certified by peer review) is the author/funder, who has granted bioRxiv a license to display the preprint in perpetuity. It is made available under aCC-BY-NC-ND 4.0 International license.

241 histone H1 lactylation may also be involved in gene-expression regulation depending on the
242 balance of Kla with acetylation.

243 In conclusion, this study indicates that a novel post-translational modification
244 called lysine lactylation occurs in the brain, and it is regulated by neuronal activity. While
245 63 candidate lactylated proteins were identified in the brain, it remains unclear whether
246 such a modification has functional significance for each protein at the cellular and behavior
247 levels, and if it does, in what brain regions and in what cell types and in what types of
248 behavioral phenotypes. It would also be interesting to explore whether protein lactylation
249 in the brain is related to the etiology and pathophysiology of neuropsychiatric disorders, as
250 are altered lactate levels in the brains of animals[3]. Further studies may reveal unknown
251 roles of lactate, linking neural activity, glycolytic metabolism, and molecular signaling
252 mediated by protein lactylation under physiological and pathophysiological conditions.
253

bioRxiv preprint doi: https://doi.org/10.1101/2021.02.02.428370; this version posted February 4, 2021. The copyright holder for this preprint (which was not certified by peer review) is the author/funder, who has granted bioRxiv a license to display the preprint in perpetuity. It is made available under aCC-BY-NC-ND 4.0 International license.

Methods

Animals

C57BL/6J mice (7–9 weeks old) were purchased from Charles River Laboratories Japan, Inc. (Hino, Japan) and Japan SLC (Shizuoka, Japan). Retired ICR mice were purchased from Chubu Kagaku Shizai Co. Ltd. (Nagoya, Japan) and Japan SLC. The mice were habituated to their environments for a week before experimentation. All animal experiments were approved by the Institutional Animal Care and Use Committee of Fujita Health University, Ibaraki University, and The National Institute of Advanced Industrial Science and Technology based on the Law for the Humane Treatment and Management of Animals and the Standards Relating to the Care and Management of Laboratory Animals and Relief of Pain. Every effort was made to minimize the number of animals used.

Cell culture

bioRxiv preprint doi: https://doi.org/10.1101/2021.02.02.428370; this version posted February 4, 2021. The copyright holder for this preprint (which was not certified by peer review) is the author/funder, who has granted bioRxiv a license to display the preprint in perpetuity. It is made available under aCC-BY-NC-ND 4.0 International license.

Embryonic C57BL/6J mice (15.5–16.5 days old) were used for primary neuron culture. The frontal cortices and hippocampi were dissected from the brains in cold HEPES-buffered, calcium and magnesium-free Hank's balanced salt solution (HBSS; 14175-103, Thermo Fisher Scientific, Waltham, MA, USA) and dissociated in HBSS containing 0.25% papain (LS003127, Worthington Biochemical Corporation, Lakewood, NJ, USA), 0.1% L-cysteine (C7352, Merck, Darmstadt, Germany), 0.1% bovine serum albumin (BSA; A2153, Merck), and 0.01% DNase I (D4263, Merck) at 37°C for 12 minutes. The enzymatic digestion was stopped by adding a plating medium (Dulbecco's modified Eagle medium, D5796, Merck, containing 10% fetal bovine serum). Tissues were dissociated by pipetting, centrifuged at room temperature for 10 minutes, and resuspended in the plating medium. Cells were counted, seeded at a density of 25,000 cells/cm^2 on culture plates or glass coverslips previously coated with 0.01% poly-L-lysine (P8920, Merck), and incubated at 37°C. After 2 hours, the plating medium was replaced by a culture medium (Neurobasal™ medium [21103-049, Thermo Fisher Scientific] containing B-27™ Supplement [17504-044, Thermo Fisher Scientific], 0.5 mM L-glutamine [G7513, Merck], and 1% penicillin-streptomycin

bioRxiv preprint doi: https://doi.org/10.1101/2021.02.02.428370; this version posted February 4, 2021. The copyright holder for this preprint (which was not certified by peer review) is the author/funder, who has granted bioRxiv a license to display the preprint in perpetuity. It is made available under aCC-BY-NC-ND 4.0 International license.

282 solution [P4333, Merck]). The culture medium was changed by one half with fresh medium
283 every 3–4 days. At 10–14 days *in vitro*, drug treatment experiments, immunocytochemical
284 analysis were conducted.
285
286 **Immunocytochemistry**
287 Cells were fixed with 4% paraformaldehyde (PFA) in phosphate-buffered saline (PBS) for 10
288 minutes, pre-incubated for 30 minutes in 5% BSA (Merck) in PBS containing 0.05% Tween-
289 20 (PBST), and then incubated for 30 minutes in PBS containing the primary antibodies:
290 rabbit polyclonal anti-lactyllysine antibody (PTM-1401, PTM Biolabs, Hangzhou, China),
291 mouse monoclonal anti-tubulin β3 (801201, BioLegend, San Diego, CA, USA), and mouse
292 monoclonal anti-glial fibrillary acidic protein antibody (G3893, Sigma-Aldrich, St Louis, MO,
293 USA). Immunoreactivity to the antigen was visualized using Alexa Fluor 488- and Alexa Fluor
294 594-conjugated secondary antibodies (Molecular Probes, Eugene, OR). Nuclear staining was
295 performed with Hoechst 33258 (Polysciences, Warrington, PA). All reactions were
296 performed at room temperature. We used a microscope (LSM 510 META; Zeiss, Göttingen,

bioRxiv preprint doi: https://doi.org/10.1101/2021.02.02.428370; this version posted February 4, 2021. The copyright holder for this preprint (which was not certified by peer review) is the author/funder, who has granted bioRxiv a license to display the preprint in perpetuity. It is made available under aCC-BY-NC-ND 4.0 International license.

297 Germany) to obtain images of the stained cells. The soma of tubulin β3-positive cells was
298 manually delineated and the signal intensity of Kla staining within the region of interest was
299 recorded using ZEN software (Zeiss). At least 200 cells from triplicate wells per condition
300 were analyzed.

301 The specificity of the Kla antibody was confirmed using dot blot analysis of lysine
302 residues with various types of modifying groups (i.e., acetyl-, crotonyl-, propionyl-, butyryl-,
303 trimethyl-, and succinyl-lysine); the antibody showed almost no cross-reactivity with these
304 modified lysine residues[1,29]. Additionally, lactate treatment dramatically increased Kla
305 immunoreactivity in human MCF-7, Hela, and MDA-MB-231 cell lines[1,29].

306

307 **Immunohistochemistry**

308 Immunohistochemical analysis was performed as previously described with some
309 modifications[30,31]. Briefly, mice were deeply anesthetized with isoflurane and transcardially
310 perfused with PBS followed by 4% PFA in PBS. The brains were dissected, immersed
311 overnight in the same fixative, and cryoprotected by sequential incubation in 10, 20, and

bioRxiv preprint doi: https://doi.org/10.1101/2021.02.02.428370; this version posted February 4, 2021. The copyright holder for this preprint (which was not certified by peer review) is the author/funder, who has granted bioRxiv a license to display the preprint in perpetuity. It is made available under aCC-BY-NC-ND 4.0 International license.

312 30% sucrose in PBS for 2–3 days each at 4°C. After cryoprotection, brains were mounted in
313 Tissue-Tek optimal cutting temperature compound (Miles, Elkhart, IN), frozen, and cut into
314 30-µm-thick coronal sections using a microtome (CM1850; Leica Microsystems, Wetzlar,
315 Germany). The sections were stored in PBS containing 0.1% sodium azide at 4°C until further
316 use. The sections were pre-incubated for 1 hour at room temperature in 5% skim milk in
317 PBST and then incubated overnight at 4°C in PBS containing the primary antibodies. We
318 used rabbit polyclonal anti-lactyllysine antibody (PTM-1401, PTM Biolabs), mouse
319 monoclonal anti-CaM Kinase II α subunit antibody (05-532, Merck), mouse monoclonal anti-
320 GAD67 antibody (MAB5406, Millipore), mouse monoclonal anti-S-100 β subunit antibody
321 (S2532, Merck), rat monoclonal anti-CD68 antibody (ab53444, abcam), and mouse
322 monoclonal anti-c-Fos antibody (sc-166940, Santa Cruz Biotechnology, Santa Cruz, CA, USA).
323 For c-Fos staining, antigen retrieval was performed by autoclave heating at 120°C for 1
324 minute in 0.01 M sodium citrate buffer prior to the blocking step. Immunoreactivity to the
325 antigen was visualized using Alexa Fluor 488- or Alexa Fluor 594-conjugated secondary
326 antibody (Molecular Probes). Nuclear staining was performed with Hoechst 33258

bioRxiv preprint doi: https://doi.org/10.1101/2021.02.02.428370; this version posted February 4, 2021. The copyright holder for this preprint (which was not certified by peer review) is the author/funder, who has granted bioRxiv a license to display the preprint in perpetuity. It is made available under aCC-BY-NC-ND 4.0 International license.

(Polysciences). We used a microscope (LSM 510 META; Zeiss) to obtain images of the stained sections. Three to seven sections from each animal were processed for semi-quantification analyses in each brain region, and the averaged values were considered as one sample. c-Fos-positive cells were counted in the indicated brain regions, manually delineated using ZEN software (Zeiss) according to the mouse brain atlas[32]. For c-Fos and Kla immunofluorescence intensity analysis in individual cells, c-Fos-positive cells were circled, and the signal intensity for each antibody within the circled areas was recorded using Zen software (Zeiss). For Kla immunofluorescence intensity, to reduce potential artifacts across sections, the values were calculated from the mean signal intensity of the entire image by subtracting background signals using Zen software (Zeiss). Semi-quantification analyses were performed in the medial PFC (approximately from 2.1 to 2.4 mm from the bregma), dorsal hippocampus, lateral habenula, and amygdala (approximately from -2.1 to -1.6 mm from the bregma), and ventral hippocampus (approximately from -3.5 to -3.8 mm from the bregma).

bioRxiv preprint doi: https://doi.org/10.1101/2021.02.02.428370; this version posted February 4, 2021. The copyright holder for this preprint (which was not certified by peer review) is the author/funder, who has granted bioRxiv a license to display the preprint in perpetuity. It is made available under aCC-BY-NC-ND 4.0 International license.

342 **STED microscopy**

343 Brain slices were doubleimmunostained as described above. Mouse monoclonal anti-
344 histone H1 antibody (sc-8030; Santa Cruz Biotechnology, Inc.) and rabbit polyclonal anti-Kla
345 antibody were the primary antibodies, and Alexa Fluor 555- and Alexa Fluor 488 conjugated
346 antibodies (Molecular Probes) were the secondary antibodies.

347 STED images were acquired with a TCS SP8 STED 3X system (Leica Microsystems,
348 Wetzlar, Germany) with 2ch HyDSMD detectors[33]. A white laser (for excitation) and a 660-
349 nm laser with a donut beam (for stimulated emission depletion) were used for STED imaging.
350 For detection of histone H1 and Kla, we used excitation wavelengths of 561 and 488 nm,
351 respectively. Raw STED images (pixel size: 20 nm) were recorded with a 93× glycerol
352 immersion objective (Leica HC PL APO 93×/1.30 GLYC motC STED W) and deconvoluted
353 using the Huygens software (SVI, Hilversum, Netherlands). The percentage of merged area
354 in a nucleus stained for both histone H1 and Kla was estimated using the ImageJ program.

355

356 **Immunoprecipitation**

bioRxiv preprint doi: https://doi.org/10.1101/2021.02.02.428370; this version posted February 4, 2021. The copyright holder for this preprint (which was not certified by peer review) is the author/funder, who has granted bioRxiv a license to display the preprint in perpetuity. It is made available under aCC-BY-NC-ND 4.0 International license.

The PFCs were dissected, snap-frozen in liquid nitrogen, and stored at -80°C until further use. Fifty microliters of Dynabeads™ Protein G solution (10007D; Thermo Fisher Scientific) was separated into low-protein absorption tubes (PROKEEP; Watson Bio Lab, Tokyo, Japan) and reacted with 2 μg of rabbit polyclonal anti-lactyllysine antibody (PTM Biolabs) or normal rabbit IgG (Cell Signaling Technology, Inc., Danvers, MA, USA). The frozen tissues were then homogenized in lysis buffer (FNN0021, Thermo Fisher Scientific). Then, 200 μL of 1-μg/μL tissue lysate was added to the bead-antibody complex and incubated with a rotation of 30 minutes at room temperature. The bead-antibody-antigen complex was then processed for mass spectrometry.

Mass spectrometry

Trypsin digestion: Bead-antibody-antigen complex was washed with 50 mM ammonium bicarbonate. The binding proteins were eluted by trypsin (Promega Corporation, Madison, WI, USA) for 1 hour at 37℃, reduced with 10 mM dithiothreitol for 30 minutes at room temperature, and alkylated with 20 mM iodoacetamide for 30 minutes at room

bioRxiv preprint doi: https://doi.org/10.1101/2021.02.02.428370; this version posted February 4, 2021. The copyright holder for this preprint (which was not certified by peer review) is the author/funder, who has granted bioRxiv a license to display the preprint in perpetuity. It is made available under aCC-BY-NC-ND 4.0 International license.

372 temperature, followed by an overnight incubation at 37°C. Digestion was stopped by adding
373 trifluoroacetic acid. The digested sample was desalted using GL-Tip SDB (GL Sciences, Tokyo,
374 Japan) and then dissolved in 20 µL of 0.1% trifluoroacetic acid.

375 *Liquid chromatograph-tandem mass spectrometer (LC-MS/MS) analysis:* The peptides were
376 analyzed using LC-MS (EASY-nLC™ 1000, Orbitrap Fusion EDT; Thermo Fisher Scientific).
377 Injected peptides were trapped on an Acclaim™ PepMap™ 100 C18 LC column (3 µm particle
378 size, 0.075 mm inner diameter × 20 mm length; Thermo Fisher Scientific) and separated on
379 an EASY-Spray LC column (3 µm particle size, 0.075 mm inner diameter × 150 mm length;
380 Thermo Fisher Scientific) with a linear gradient of 0–35% acetonitrile with 0.1% formic acid
381 over 60 minutes at a flow rate of 300 nL/minute. Data acquisition was performed using
382 Xcalibur™ (Thermo Fisher Scientific). Full MS spectra (m/z 375–1500) were acquired at a
383 resolution of 120,000. The most intense precursor ions were selected for collision-induced
384 fragmentation in the linear ion trap at a normalized collision energy of 35%. Dynamic
385 exclusion was employed within 60 seconds to prevent repetitive selection of peptides.

bioRxiv preprint doi: https://doi.org/10.1101/2021.02.02.428370; this version posted February 4, 2021. The copyright holder for this preprint (which was not certified by peer review) is the author/funder, who has granted bioRxiv a license to display the preprint in perpetuity. It is made available under aCC-BY-NC-ND 4.0 International license.

386 *Data analysis:* Raw data were analyzed using Proteome Discoverer™ (version 2.2, Thermo
387 Fisher Scientific) with the Mascot search engine (version 2.6.1, Matrix Science Ltd., London,
388 UK) against the Swiss-Prot database. The search parameters were as follows: mass
389 tolerances in MS and MS/MS, 10 ppm and 0.6 Da; maximum missed cleavages allowed, 2.
390 Methionine oxidation and N-acetylation were set as variable modifications, and cysteine
391 carbamidomethylation was set as a fixed modification. A target-decoy database search was
392 used to estimate the false-positive ratio for peptide identification; the false discovery rate
393 was set at 1%.

394

395 **Western blot analysis**

396 Western blot analysis was performed as previously described, with some modifications[30,31].
397 Tissues from the brain and peripheral organs were collected from adult c57BL6/J mice,
398 snap-frozen in liquid nitrogen, and stored at -80°C until further use. Peritoneal cavity cells
399 were collected from adult C67BL/6J mice and used as a macrophage sample. Tissues and
400 cultured cells were homogenized in lysis buffer (MCL1, Merck). Protein homogenates were

bioRxiv preprint doi: https://doi.org/10.1101/2021.02.02.428370; this version posted February 4, 2021. The copyright holder for this preprint (which was not certified by peer review) is the author/funder, who has granted bioRxiv a license to display the preprint in perpetuity. It is made available under aCC-BY-NC-ND 4.0 International license.

401 separated with gel electrophoresis using NuPAGE™ 4–12% Bis-Tris gels (Thermo Fisher
402 Scientific) and transferred to polyvinylidene difluoride membranes. Membranes were
403 preincubated in 5% skim milk in Tris-buffered saline with 0.05% Tween® 20 (TBST) for 1 hour
404 and incubated for 2 hours in primary antibody, rabbit polyclonal anti-lactyllysine antibody
405 (PTM Biolabs), or mouse monoclonal anti-β-actin antibody (A5316, Merck) diluted in TBST.
406 They were then incubated for 1 hour with a secondary antibody conjugated with
407 horseradish peroxidase (sc-2357, anti-rabbit IgG; sc-516102, anti-mouse IgG; Santa Cruz
408 Biotechnology) diluted with TBST. All reactions were performed at room temperature.
409 Immunoreactivity was visualized with a chemiluminescence detection regent (ImmunoStar
410 LD, 292-69903; FUJIFILM Wako Pure Chemical Corporation, Osaka, Japan) and
411 photographed with a luminescent image analyzer (LAS-4000 mini; GE Healthcare,
412 Buckinghamshire, UK).

413

414 **Electroconvulsive stimulation**

bioRxiv preprint doi: https://doi.org/10.1101/2021.02.02.428370; this version posted February 4, 2021. The copyright holder for this preprint (which was not certified by peer review) is the author/funder, who has granted bioRxiv a license to display the preprint in perpetuity. It is made available under aCC-BY-NC-ND 4.0 International license.

The experimental mice were briefly anesthetized with isoflurane, and bilateral electroconvulsive stimulation (ECS; current: 25 mA; shock duration: 1 s; frequency: 100 pulses/sec; pulse width: 0.5 msec) was administered via ear clip electrodes with a pulse generator (ECT Unit; Ugo Basile, Gemonio, VA, Italy)[34]. Control mice were handled similarly, except that they were not administered ECS.

Chronic SDS

Condition 1

SDS serves as a preclinical model of chronic stress[35,36]. We performed chronic social defeat stress in mice at Fujita Health University, as previously described[36].

Screening of aggressor ICR mice: Retired ICR breeders were screened for aggressive behavior for 3 consecutive days. They were individually housed in a clear rectangular hamster cage (26.7 cm [width] × 48.3 cm [depth] × 15.2 cm [height]; Allentown Caging Equipment, Allentown, NJ, USA) equipped with a clear perforated Plexiglass divider (0.6 cm

bioRxiv preprint doi: https://doi.org/10.1101/2021.02.02.428370; this version posted February 4, 2021. The copyright holder for this preprint (which was not certified by peer review) is the author/funder, who has granted bioRxiv a license to display the preprint in perpetuity. It is made available under aCC-BY-NC-ND 4.0 International license.

429 [width] × 45.7 cm [depth] × 15.2 cm [height]; Chubu Kagaku Shizai [custom order]) and a
430 steel-wire top (Allentown Caging Equipment).

431 *Chronic SDS*: Experimental C57BL/6J mice were placed in the compartment containing an
432 aggressor ICR mouse and were exposed to social defeat for 10 minutes. During this period,
433 the experimental mice generally displayed submissive behaviors. They were then
434 transferred to the other compartment of the aggressor's cage, allowing sensory interaction
435 with the intruder C57BL/6J mouse and resident ICR aggressor mouse for approximately 24
436 hours (cohabitation housing condition). This procedure was repeated for 10 consecutive
437 days, with each experimental C57BL/6J mouse being exposed to a novel ICR aggressor each
438 day to prevent habituation. Control C57BL/6J mice were placed in pairs in an identical home
439 cage separated by a perforated divider. The control animals were rotated to a new cage
440 compartment daily and allowed to interact with a novel mouse of the same strain. Following
441 the last defeat session, all C57BL/6J mice were singly housed in standard mouse cages.
442 Twenty-four hours after the last defeat session, a social avoidance test and other behavioral

bioRxiv preprint doi: https://doi.org/10.1101/2021.02.02.428370; this version posted February 4, 2021. The copyright holder for this preprint (which was not certified by peer review) is the author/funder, who has granted bioRxiv a license to display the preprint in perpetuity. It is made available under aCC-BY-NC-ND 4.0 International license.

443 tests were conducted as described. Brain sampling was performed 8 days after the last

444 defeat session. *Condition 1* was used for OX-treatment experiments.

445

446 *Condition 2*

447 The experiment was performed at Fujita Health University, as described in *Condition 1*,

448 except that the intruder C57BL/6J mice were individually housed in separate cages, away

449 from ICR aggressor mice, after the 10-minute-aggression (separation housing condition). As

450 in *Condition 1*, brain sampling was performed 8 days after the last defeat session.

451

452 *Condition 3*

453 The experiment was performed at Ibaraki University, as previously described[37]. The intruder

454 C57BL/6J mice were exposed to sensory interaction with a resident ICR aggressor mouse in

455 the other compartment of the aggressor's cage for approximately 24 hours (cohabitation

bioRxiv preprint doi: https://doi.org/10.1101/2021.02.02.428370; this version posted February 4, 2021. The copyright holder for this preprint (which was not certified by peer review) is the author/funder, who has granted bioRxiv a license to display the preprint in perpetuity. It is made available under aCC-BY-NC-ND 4.0 International license.

456 housing condition). Twenty-four hours after the last defeat session, a social avoidance test
457 was conducted [37]. Brain sampling was performed 2 days after the last defeat session.
458
459 **Drug treatment**
460 Twenty minutes prior to each defeat session, the mice were intraperitoneally administered
461 sodium oxamate (OX; 1 g/kg; O2751, Sigma-Aldrich, Tokyo, Japan) or sodium L-lactate (1
462 g/kg; L-7022, Sigma-Aldrich). They were administered the same amount of saline as the
463 control. OX is an inhibitor of lactate dehydrogenase (LDH) activity in the central nervous
464 system[13,14]. The dose of OX that we used was previously shown to be effective in
465 suppressing seizures in a mouse model of epilepsy[14]. The dose of sodium L-lactate that we
466 used was previously shown to exert antidepressant-like effects in a corticosterone-induced
467 chronic stress model in mice[7].
468
469 **Behavioral tests**

bioRxiv preprint doi: https://doi.org/10.1101/2021.02.02.428370; this version posted February 4, 2021. The copyright holder for this preprint (which was not certified by peer review) is the author/funder, who has granted bioRxiv a license to display the preprint in perpetuity. It is made available under aCC-BY-NC-ND 4.0 International license.

Most of the behavioral tests were performed as described elsewhere[38–41], unless otherwise noted.

Social interaction test: Social interaction was tested 1 day after the last defeat session as previously described[36], with minor modifications. We used an open field chamber (40 cm (width) × 40 cm (depth) × 30 cm (height); O'HARA & Co., Tokyo, Japan) and a wire mesh cage (10.5 cm (width) × 6.5 cm (depth) × 29 cm (height); O'HARA & Co.) to enclose the ICR aggressor mouse. The ICR aggressor mouse that is novel to the defeated C57BL/6J mouse was used. Each social interaction test was composed of two 150-second phases: the ICR aggressor mouse is absent and present in the interaction zone for the first and second phase, respectively. An identical, empty wire mesh cage was placed for the first phase testing. A 13.7 cm × 23.6 cm rectangular zone including the wire mesh cage was defined as the social interaction zone. Mouse behaviors were video-monitored, and the trajectory of mouse ambulation, distance traveled, and time spent in the interaction zone for all test phases were automatically determined using ImageSI (see "Image analysis"). A social interaction

bioRxiv preprint doi: https://doi.org/10.1101/2021.02.02.428370; this version posted February 4, 2021. The copyright holder for this preprint (which was not certified by peer review) is the author/funder, who has granted bioRxiv a license to display the preprint in perpetuity. It is made available under aCC-BY-NC-ND 4.0 International license.

ratio was calculated by dividing the time spent in the interaction zone when the target was present by the time spent in the interaction zone when the target was absent. A social interaction ratio of 1 was considered the threshold for dividing defeated mice into the susceptible and resilient groups.

Light/dark transition test: A light/dark transition test was conducted as previously described[38–42]. The apparatus consisted of a cage (42 cm (width) × 21 cm (depth) × 25 cm (height)) divided into two sections of equal size by a partition with a door (O'HARA & Co.). One chamber was brightly illuminated (390 lux), whereas the other chamber was dark (2 lux). Mice were placed into the dark chamber and allowed to move freely between the two chambers with the door open for 10 minutes. The total number of transitions, latency to first enter the lit chamber, distance traveled, and time spent in each chamber were recorded using ImageLD (see "Image analysis").

bioRxiv preprint doi: https://doi.org/10.1101/2021.02.02.428370; this version posted February 4, 2021. The copyright holder for this preprint (which was not certified by peer review) is the author/funder, who has granted bioRxiv a license to display the preprint in perpetuity. It is made available under aCC-BY-NC-ND 4.0 International license.

499 *Open field test*: The apparatus was a transparent square cage (42 cm (width) × 42 cm (depth)
500 × 30 cm (height)) equipped with infrared photobeam sensors (VersaMax; Accuscan
501 Instruments, Columbus, OH, USA) with a white floor[38–41]. The center of the floor was
502 illuminated at 100 lux. Each mouse was placed in the corner of the cage. The total distance
503 traveled (cm), vertical activity (rearing measured by counting the number of photobeam
504 interruptions), time spent in the center area (20 cm × 20 cm), and stereotypic counts
505 (defined by the number of breaks of the same beam) were recorded for 30 minutes using
506 the VersaMax system.

507

508 *Porsolt forced-swim test*: A Plexiglas cylinder (20 cm height × 11.4 cm diameter; O'HARA &
509 Co.) filled with water (21–23 °C) up to a height of 8 cm was placed in a white plastic chamber
510 (32 cm (width) × 44 cm (depth) × 49 cm (height); O'HARA & Co.) [38–41]. Mice were placed into
511 the cylinder, and both immobility and distance traveled were recorded over a 10-minute
512 test period. The test was conducted for 2 consecutive two days, and the results of the first
513 trial are shown. Images were captured at two frames per second. For each pair of successive

bioRxiv preprint doi: https://doi.org/10.1101/2021.02.02.428370; this version posted February 4, 2021. The copyright holder for this preprint (which was not certified by peer review) is the author/funder, who has granted bioRxiv a license to display the preprint in perpetuity. It is made available under aCC-BY-NC-ND 4.0 International license.

514 frames, the amount of area (pixels) in which the mouse moved was measured. When the
515 amount of area was below a certain threshold, mouse behavior was classified as “immobile.”
516 When the amount of area equaled or exceeded the threshold, the mouse was classified as
517 “moving”. The optimal threshold to judge movment was determined by adjusting it to the
518 amount of immobility measured by human observation. Immobility lasting for less than 2
519 seconds was not included in the analysis. Data acquisition and analysis were performed
520 automatically, using ImagePS/TS (see “Image analysis”).

521

522 *Tail suspension test*: Each mouse was suspended 30 cm above the floor by the tail in a white
523 plastic chamber (41cm (width) × 31 cm (depth) × 41 cm (height); O’Hara & Co.)[38–41]. The
524 behavior was recorded for 10 minutes. Images were captured through a video camera, and
525 immobility was measured. Similar to the Porsolt forced swim test mentioned above,
526 immobility was judged using ImagePS/TS (see “Image analysis”) according to a certain
527 threshold. Immobility lasting <2 seconds was not included in the analysis.

528

bioRxiv preprint doi: https://doi.org/10.1101/2021.02.02.428370; this version posted February 4, 2021. The copyright holder for this preprint (which was not certified by peer review) is the author/funder, who has granted bioRxiv a license to display the preprint in perpetuity. It is made available under aCC-BY-NC-ND 4.0 International license.

529 *Sucrose preference test*: C57BL/6J mice were subjected to a two-bottle choice test, in which
530 mice were provided with a bottle containing water and a second bottle containing 1%
531 sucrose solution, with the left/right positions of the bottles counterbalanced across groups
532 [39,40]. The mice were habituated to a two-bottle condition during all the experimental period.
533 Sucrose preference during 4-hour in the test day was calculated as the percentage of
534 sucrose preference = 100 × {[sucrose intake (g)]/(sucrose intake (g) + water intake (g)]).
535
536 *Locomotor activity monitoring in the home cage*: Locomotor activity monitoring in the home
537 cage was performed as previously described[30,41]. A system that automatically analyzes the
538 locomotor activity of mice in their home cage was used[43]. The system contains a home cage
539 (29 cm (width) × 18 cm (depth) × 12 cm (height)) and filtered cage top, separated by a 13-
540 cm-high metal stand containing an infrared video camera, attached to the top of the stand.
541 Each mouse was individually housed in each home cage, and their locomotor activity was
542 monitored for 6 days. Mice were allowed to habituate to the test apparatus, and hence, the

bioRxiv preprint doi: https://doi.org/10.1101/2021.02.02.428370; this version posted February 4, 2021. The copyright holder for this preprint (which was not certified by peer review) is the author/funder, who has granted bioRxiv a license to display the preprint in perpetuity. It is made available under aCC-BY-NC-ND 4.0 International license.

data of the latter 3 days were analyzed. Distance traveled was measured automatically using ImageHA (see "Image analysis").

Image analysis: For the social interaction test, light/dark transition test, Porsolt forced swim test, and tail suspension test, image analysis programs (ImageSI/LD/PS/TS/HA) were used to automatically analyze mouse behaviors. The application programs, based on the public domain ImageJ program (developed by Wayne Rasband at the National Institute of Mental Health, Bethesda), were developed and modified for each test by Tsuyoshi Miyakawa. ImageLD program can be freely downloaded from the website of the "Mouse Phenotype Database" (http://www.mouse-phenotype.org/)[44].

Measurements of brain lactate levels and pH

In the *in vivo* experiments, the whole brain was used to measure tissue pH and lactate levels as previously described[3]. Briefly, snap-frozen tissues were homogenized in ice-cold distilled

bioRxiv preprint doi: https://doi.org/10.1101/2021.02.02.428370; this version posted February 4, 2021. The copyright holder for this preprint (which was not certified by peer review) is the author/funder, who has granted bioRxiv a license to display the preprint in perpetuity. It is made available under aCC-BY-NC-ND 4.0 International license.

557 H_2O (5 mL per 500 mg of tissue). The pH of the homogenates was measured using a pH
558 meter (LAQUA F-72, HORIBA, Ltd., Kyoto, Japan) equipped with a Micro ToupH electrode
559 (9618S-10D, HORIBA, Ltd.) after a three-point calibration at pH 4.0, 7.0, and 9.0. Following,
560 the concentration of lactate in the homogenates was determined using a multi-assay
561 analyzer (GM7 Micro-Stat; Analox Instruments Ltd., London, UK) after calibration with an
562 8.0-M standard lactate solution (GMRD-103, Analox Instruments). A 20-µL aliquot of
563 centrifuged supernatant was used for the measurement. In the *in vitro* experiments, lactate
564 concentrations of the cultured cells and culture supernatant were measured using the
565 lactate colorimetric assay kit II (K627-100; BioVision, Milpitas, CA, USA). Light transmittance
566 was measured at a wavelength of 450 nm using a spectrophotometer (DU730; Beckman
567 Coulter, Tokyo, Japan).
568
569 **Statistical analysis**
570 The data were analyzed by Student's t-test, one-way analysis of variance (ANOVA), two-way
571 ANOVA, followed by Tukey's honestly significant difference post-hoc test, or linear

bioRxiv preprint doi: https://doi.org/10.1101/2021.02.02.428370; this version posted February 4, 2021. The copyright holder for this preprint (which was not certified by peer review) is the author/funder, who has granted bioRxiv a license to display the preprint in perpetuity. It is made available under aCC-BY-NC-ND 4.0 International license.

572 regression analysis using R version 3.5.2 or SAS Studio software version 9.4 (SAS Institute

573 Inc., Cary, NC, USA).

574

575 **Data availability**

576 The original blot images are provided in Extended data figures. The full statistical results are

577 provided in Extended data tables.

578

579 **References**

580 1. Zhang, D. *et al.* Metabolic regulation of gene expression by histone lactylation.
581 *Nature* **574**, 575–580 (2019).
582 2. Magistretti, P. J. & Allaman, I. Lactate in the brain: from metabolic end-product
583 to signalling molecule. *Nat. Rev. Neurosci.* **19**, 235–249 (2018).
584 3. Hagihara, H. *et al.* Decreased brain pH as a shared endophenotype of psychiatric
585 disorders. *Neuropsychopharmacology* **43**, 459–468 (2018).
586 4. Hagihara, H. *et al.* Systematic analysis of brain lactate and pH levels in 65 animal
587 models related to neuropsychiatric conditions. *bioRxiv* 2021.02.02.428362 (2021).
588 5. Irizarry-Caro, R. A. *et al.* TLR signaling adapter BCAP regulates inflammatory to
589 reparatory macrophage transition by promoting histone lactylation. *Proc. Natl. Acad. Sci.*
590 **117**, 30628–30638 (2020).

bioRxiv preprint doi: https://doi.org/10.1101/2021.02.02.428370; this version posted February 4, 2021. The copyright holder for this preprint (which was not certified by peer review) is the author/funder, who has granted bioRxiv a license to display the preprint in perpetuity. It is made available under aCC-BY-NC-ND 4.0 International license.

591 6. Cui, H. *et al.* Lung myofibroblasts promote macrophage profibrotic activity
592 through lactate-induced histone lactylation. *Am. J. Respir. Cell Mol. Biol.* **64**, 115–125
593 (2020).
594 7. Carrard, A. *et al.* Peripheral administration of lactate produces antidepressant-
595 like effects. *Mol. Psychiatry* (2016) doi:10.1038/mp.2016.179.
596 8. Busnello, J. V. *et al.* Acute and chronic electroconvulsive shock in rats: Effects on
597 peripheral markers of neuronal injury and glial activity. *Life Sci.* **78**, 3013–3017 (2006).
598 9. Díaz-García, C. M. *et al.* Neuronal stimulation triggers neuronal glycolysis and
599 not lactate uptake. *Cell Metab.* **26**, 361-374.e4 (2017).
600 10. Lazeyras, F. *et al.* MRI, 1H-MRS, and functional MRI during and after prolonged
601 nonconvulsive seizure activity. *Neurology* **55**, 1677–1682 (2000).
602 11. Najm, I. M. *et al.* Temporal changes in proton MRS metabolites after kainic acid-
603 induced seizures in rat brain. *Epilepsia* **38**, 87–94 (1997).
604 12. Oses, J. P. *et al.* Sustained elevation of cerebrospinal fluid glucose and lactate
605 after a single seizure does not parallel with mitochondria energy production. *Epilepsy Res.*
606 **152**, 35–41 (2019).
607 13. Lam, T. K. T., Gutierrez-Juarez, R., Pocai, A. & Rossetti, L. Regulation of blood
608 glucose by hypothalamic pyruvate metabolism. *Science* **309**, 943–947 (2005).
609 14. Sada, N., Lee, S., Katsu, T., Otsuki, T. & Inoue, T. Targeting LDH enzymes with a
610 stiripentol analog to treat epilepsy. *Science* **347**, 1362–1367 (2015).
611 15. Bullitt, E. Expression of C-fos-like protein as a marker for neuronal activity
612 following noxious stimulation in the rat. *J. Comp. Neurol.* **296**, 517–530 (1990).
613 16. Bullitt, E., Lee, C. L., Light, A. R. & Willcockson, H. The effect of stimulus duration
614 on noxious-stimulus induced c-fos expression in the rodent spinal cord. *Brain Res.* **580**,
615 172–179 (1992).
616 17. Kollack-Walker, Don, Watson, & Akil. Differential Expression of c- *fos* mRNA
617 Within Neurocircuits of Male Hamsters Exposed to Acute or Chronic Defeat. *J.*
618 *Neuroendocrinol.* **11**, 547–559 (1999).
619 18. Martinez, M., Calvo-Torrent, A. & Herbert, J. Mapping brain response to social
620 stress in rodents with c-fos expression: A review. *Stress* **5**, 3–13 (2002).

bioRxiv preprint doi: https://doi.org/10.1101/2021.02.02.428370; this version posted February 4, 2021. The copyright holder for this preprint (which was not certified by peer review) is the author/funder, who has granted bioRxiv a license to display the preprint in perpetuity. It is made available under aCC-BY-NC-ND 4.0 International license.

621 19. Matsuda, S. *et al.* Persistent c-fos expression in the brains of mice with chronic
622 social stress. *Neurosci. Res.* **26**, 157–170 (1996).
623 20. Ma, M. *et al.* Adjunctive treatment of brexpiprazole with fluoxetine shows a
624 rapid antidepressant effect in social defeat stress model: Role of BDNF-TrkB signaling. *Sci.*
625 *Rep.* **6**, 1–12 (2016).
626 21. Yang, B. *et al.* Comparison of R-ketamine and rapastinel antidepressant effects
627 in the social defeat stress model of depression. *Psychopharmacology (Berl.)* **233**, 3647–
628 3657 (2016).
629 22. Huang, D. W., Sherman, B. T. & Lempicki, R. A. Systematic and integrative
630 analysis of large gene lists using DAVID bioinformatics resources. *Nat. Protoc.* **4**, 44–57
631 (2009).
632 23. Huang, D. W., Sherman, B. T. & Lempicki, R. A. Bioinformatics enrichment tools:
633 paths toward the comprehensive functional analysis of large gene lists. *Nucleic Acids Res.*
634 **37**, 1–13 (2009).
635 24. Martinez, M., Phillips, P. J. & Herbert, J. Adaptation in patterns of c-fos
636 expression in the brain associated with exposure to either single or repeated social stress
637 in male rats. *Eur. J. Neurosci.* **10**, 20–33 (1998).
638 25. Gaffney, D. O. *et al.* Non-enzymatic lysine lactoylation of glycolytic enzymes. *Cell*
639 *Chem. Biol.* **27**, 206-213.e6 (2020).
640 26. Andrés, M., García-Gomis, D., Ponte, I., Suau, P. & Roque, A. Histone H1 post-
641 translational modifications: update and future perspectives. *Int. J. Mol. Sci.* **21**, 5941
642 (2020).
643 27. Wisniewski, J. R., Zougman, A., Krüger, S. & Mann, M. Mass spectrometric
644 mapping of linker histone H1 variants reveals multiple acetylations, methylations, and
645 phosphorylation as well as differences between cell culture and tissue. *Mol. Cell.*
646 *Proteomics MCP* **6**, 72–87 (2007).
647 28. Kamieniarz, K. *et al.* A dual role of linker histone H1.4 Lys 34 acetylation in
648 transcriptional activation. *Genes Dev.* **26**, 797–802 (2012).
649 29. Anti-L-lactyllysine rabbit pAb. *PTM BIO*
650 https://www.ptmbiolabs.com/product/anti-lactyllysine-rabbit-pab/ (2019).

bioRxiv preprint doi: https://doi.org/10.1101/2021.02.02.428370; this version posted February 4, 2021. The copyright holder for this preprint (which was not certified by peer review) is the author/funder, who has granted bioRxiv a license to display the preprint in perpetuity. It is made available under aCC-BY-NC-ND 4.0 International license.

651 30. Hagihara, H. *et al.* Circadian gene circuitry predicts hyperactive behavior in a
652 mood disorder mouse model. *Cell Rep.* **14**, 2784–2796 (2016).
653 31. Hagihara, H., Ohira, K., Toyama, K. & Miyakawa, T. Expression of the AMPA
654 receptor subunits GluR1 and GluR2 is associated with granule cell maturation in the
655 dentate gyrus. *Front. Neurosci.* **5**, (2011).
656 32. Franklin, K. B. J. & Paxinos, G. *The Mouse Brain in Stereotaxic Coordinates*.
657 (Academic Press Inc.. San Diego., 1997).
658 33. Tanaka, M. *et al.* Fascin in lamellipodia contributes to cell elasticity by
659 controlling the orientation of filamentous actin. *Genes Cells* **24**, 202–213 (2019).
660 34. Imoto, Y., Segi-Nishida, E., Suzuki, H. & Kobayashi, K. Rapid and stable changes in
661 maturation-related phenotypes of the adult hippocampal neurons by electroconvulsive
662 treatment. *Mol. Brain* **10**, 8 (2017).
663 35. Krishnan, V., Berton, O. & Nestler, E. The use of animal models in psychiatric
664 research and treatment. *Am. J. Psychiatry* **165**, 1109 (2008).
665 36. Golden, S. A., Covington, H. E., Berton, O. & Russo, S. J. A standardized protocol
666 for repeated social defeat stress in mice. *Nat. Protoc.* **6**, 1183–1191 (2011).
667 37. Goto, T. *et al.* Subchronic and mild social defeat stress accelerates food intake
668 and body weight gain with polydipsia-like features in mice. *Behav. Brain Res.* **270**, 339–348
669 (2014).
670 38. Shoji, H. & Miyakawa, T. Age-related behavioral changes from young to old age
671 in male mice of a C57BL/6J strain maintained under a genetic stability program.
672 *Neuropsychopharmacol. Rep.* **39**, 100–118 (2019).
673 39. Shoji, H. & Miyakawa, T. Increased depression-related behavior during the
674 postpartum period in inbred BALB/c and C57BL/6 strains. *Mol. Brain* **12**, 70 (2019).
675 40. Shoji, H. & Miyakawa, T. Differential effects of stress exposure via two types of
676 restraint apparatuses on behavior and plasma corticosterone level in inbred male
677 BALB/cAJcl mice. *Neuropsychopharmacol. Rep.* **40**, 73–84 (2020).
678 41. Nakajima, R. *et al.* Comprehensive behavioral analysis of heterozygous Syngap1
679 knockout mice. *Neuropsychopharmacol. Rep.* **39**, 223–237 (2019).

bioRxiv preprint doi: https://doi.org/10.1101/2021.02.02.428370; this version posted February 4, 2021. The copyright holder for this preprint (which was not certified by peer review) is the author/funder, who has granted bioRxiv a license to display the preprint in perpetuity. It is made available under aCC-BY-NC-ND 4.0 International license.

680 42. Takao, K. & Miyakawa, T. Light/dark transition test for mice. *J. Vis. Exp. JoVE* 104
681 (2006) doi:10.3791/104.
682 43. Miyakawa, T. *et al.* Conditional calcineurin knockout mice exhibit multiple
683 abnormal behaviors related to schizophrenia. *Proc. Natl. Acad. Sci. U. S. A.* **100**, 8987–
684 8992 (2003).
685 44. Hattori, S., Okumura, Y., Takao, K., Yamaguchi, Y. & Miyakawa, T. Open source
686 code for behavior analysis in rodents. *Neuropsychopharmacol. Rep.* **39**, 67–69 (2019).

687

688 **Acknowledgements**

689 We thank Giovanni Sala for invaluable comments on statistics. We also thank Tamaki
690 Murakami, Chikako Ozeki, Wakako Hasegawa, Yumiko Mobayashi, Yoko Kagami, Harumi
691 Mitsuya, Yoshihiro Takamiya, Satoko Hattori and Miho Tanaka for their technical assistance.
692 This work was supported by MEXT KAKENHI Grant Number JP16H06462, JP17H06417, and
693 JP17H06413, MEXT Promotion of Distinctive Joint Research Center Program Grant Number
694 JPMXP0618217663, JSPS KAKENHI Grant Number JP20H00522, JP18K07378, JP19K06502,
695 and JP16H06276 (AdAMS), and AMED Strategic Research Program for Brain Sciences Grant
696 Number JP18dm0107101.

697

698 **Author information**

bioRxiv preprint doi: https://doi.org/10.1101/2021.02.02.428370; this version posted February 4, 2021. The copyright holder for this preprint (which was not certified by peer review) is the author/funder, who has granted bioRxiv a license to display the preprint in perpetuity. It is made available under aCC-BY-NC-ND 4.0 International license.

699 **Contributions.** H.H. and T.M. designed experiments. H.H. wrote the manuscript. K.N., K.K.,

700 and T.M. helped draft the manuscript. H.H., H.S., H.O., and A.T. performed the behavioral

701 tests and analyzed the data. K. K. and M. N. performed STED microscopy analysis. T.M.

702 supervised all aspects of the present study. All authors have approved the final manuscript.

703 **Corresponding authors.** Correspondence to Tsuyoshi Miyakawa.

704

705 **Ethics declarations**

706 The authors declare no competing interests.

bioRxiv preprint doi: https://doi.org/10.1101/2021.02.02.428370; this version posted February 4, 2021. The copyright holder for this preprint (which was not certified by peer review) is the author/funder, who has granted bioRxiv a license to display the preprint in perpetuity. It is made available under aCC-BY-NC-ND 4.0 International license.

Figure legends

Figure 1. Protein lactylation induced by exogenous lactate in brain cells. (a) Western blot images of lactylated lysine (Kla) in mouse tissues/cells (hippocampus (HIP), cerebral cortex (CX), and resident macrophages (MP). Entire membrane images are provided in the Extended Data Fig. 1. (b) Double immunostaining for Kla and the neuronal marker βIII-tubulin in primary cultured cortical neurons (10 days in vitro, DIV). Scale bar: 20 µm. (c, d) Kla levels in primary cultured cortical neurons (10 DIV) examined 30 minutes after treatment with lactate (25 mM, +) and/or 4-CIN (0.01 mM, +; 1 mM, ++) using immunocytochemistry. Arrow in (c) indicates the sampling time point. At least 200 cells were examined for each condition. Statistical results are provided in Extended Data Table 4. (e) Glial fibrillary acidic protein (GFAP) and Kla double immunostaining at 10 DIV in culture. Open arrows indicate GFAP-positive astrocyte-like cells. Solid arrows indicate GFAP-negative neuronal cells. Scale bar: 50 µm. (f–h) Mice were intraperitoneally injected with 1 g/kg lactate or saline, once daily for 21 days. (g) Kla immunostaining images of the prefrontal cortices (PFCs) of control and lactate-treated mice. Scale bar: 100 µm. (h) Bar

bioRxiv preprint doi: https://doi.org/10.1101/2021.02.02.428370; this version posted February 4, 2021. The copyright holder for this preprint (which was not certified by peer review) is the author/funder, who has granted bioRxiv a license to display the preprint in perpetuity. It is made available under aCC-BY-NC-ND 4.0 International license.

722 graph showing Kla immunoreactivity levels of the PFC of control and lactate-treated mice
723 (P = 0.022, n = 7, 6). (i) Mouse PFC: Double immunostaining images of Kla and the
724 glutamatergic neuron marker Camk2a (upper left panel), the GABAergic neuron marker
725 GAD67 (upper right panel), the astrocyte marker S100b (lower left panel), and the microglial
726 marker CD68 (lower right panel). Scale bar: 25 μm.

727

728 **Figure 2. Neuronal excitation stimulates protein lactylation in neurons.** (a–c) Primary
729 cultured cortical neurons (10 DIV) were treated with potassium chloride (KCl), with or
730 without sodium oxamate (OX). Arrows indicate sampling time points (a). Cultured neurons
731 were treated with KCl (100 mM) and lactate concentrations were measured in the culture
732 supernatant (upper panel, b) and cell lysate (lower panel, b). *P < 0.05, one-way analysis of
733 variance (ANOVA) followed by post-hoc pairwise comparisons. N = 5 for each condition.
734 Statistical results are provided in the Extended Data Table 5. (c) Results of Kla
735 immunostaining analysis of cultured neurons expressing βIII-tubulin treated with KCl [10
736 mM (+) or 100 mM (++)] and OX [20 mM (+)] (c) At least 300 cells were examined for each

bioRxiv preprint doi: https://doi.org/10.1101/2021.02.02.428370; this version posted February 4, 2021. The copyright holder for this preprint (which was not certified by peer review) is the author/funder, who has granted bioRxiv a license to display the preprint in perpetuity. It is made available under aCC-BY-NC-ND 4.0 International license.

737 condition. **P < 0.01; ##P < 0.01 compared to the KCl/OX condition; one-way ANOVA
738 followed by post-hoc pairwise comparisons (Extended Data Table 6). (d, e) Brain lactate
739 levels in mice treated with electroconvulsive stimulation (ECS) (N = 8 mice for each
740 condition). ##P < 0.01 compared to control; one-way ANOVA followed by post-hoc pairwise
741 comparisons (Extended Data Table 7). (f–h) Kla in the mouse brain treated with ECS. Adult
742 mice were treated with ECS 30 minutes after treatment with OX, α-cyano-4-
743 hydroxycinnamate (4-CIN), or saline. Brain sampling was performed 1 hour after ECS
744 treatment (arrow, f). Immunostaining images of Kla in the prefrontal cortex (PFC). Scale bar:
745 100 μm (g). Graph showing Kla immunoreactivity in the PFCs of the mice (h). #P < 0.05
746 compared to ECS-/OX-/4-CIN-, $P < 0.05 compared to ECS+/OX-/4-CIN-; one-way ANOVA
747 followed by post-hoc pairwise comparisons. N = 6–7 mice for each condition (Extended Data
748 Table 8). (i) Kla and c-Fos double immunostaining images of the mouse PFC at 1 hour after
749 an ECS. Open and solid arrowheads indicate cells with low and high levels of Kla + c-Fos,
750 respectively. Scale bar: 50 μm. (j) Scatterplot showing a correlation between Kla and c-Fos
751 immunoreactivity in individual cells in the PFC (represented as Z-score transformed values).

bioRxiv preprint doi: https://doi.org/10.1101/2021.02.02.428370; this version posted February 4, 2021. The copyright holder for this preprint (which was not certified by peer review) is the author/funder, who has granted bioRxiv a license to display the preprint in perpetuity. It is made available under aCC-BY-NC-ND 4.0 International license.

752 Data from 543 cells from 15 mice in four different conditions (Extended Data Fig. 4) are
753 integrated in the graph.
754
755 **Figure 3. Social stress induces protein lactylation in the brain.** (a–c) Mice were exposed to
756 repeated social defeat stress, with or without sodium oxamate injections and then analyzed
757 by a series of behavioral tests (a). Arrow in (a) indicates the sampling time point. FS: Porsolt
758 forced swim test; LD: light-dark transition test; OF: open field test; OX: sodium oxamate; SA:
759 social avoidance test; SDS: social defeat stress; SP: sucrose preference test; TS: tail
760 suspension test. (b) Social avoidance test. (c) Brain lactate levels in the three groups of mice.
761 N = 10–14 mice for each condition. Statistical results are provided in the Extended Data
762 Table 9 and 10, respectively. (d) Correlation matrix showing correlation coefficients
763 between behavioral measures and brain lactate levels in control and socially defeated mice.
764 (e, f) Brain sampling for immunohistochemical analysis was performed using another set of
765 mice exposed to SDS with or without OX injection. (e) HC: home cage locomotor activity
766 monitoring test. (f) Immunostaining images of Kla and bar graph showing Kla

bioRxiv preprint doi: https://doi.org/10.1101/2021.02.02.428370; this version posted February 4, 2021. The copyright holder for this preprint (which was not certified by peer review) is the author/funder, who has granted bioRxiv a license to display the preprint in perpetuity. It is made available under aCC-BY-NC-ND 4.0 International license.

767 immunoreactivity in the prefrontal cortex (PFC). Scale bar: 100 μm. **P < 0.01, one-way
768 analysis of variance followed by post-hoc pairwise comparisons; N = 6 mice for each
769 condition (Extended Data Table 11). (g) Immunostaining images of c-Fos in the PFC. (h) Bar
770 graphs showing c-Fos-positive cells in the PFC (Extended Data Table 12). Mice in the home
771 cage group were sampled immediately after being removed from the home cage. Mice in
772 the OF group were sampled after a 2-hour exposure to the open field. (i–k) Scatterplots
773 showing correlations between Kla immunoreactivity and c-Fos expression in the PFC and (i)
774 the social interaction ratio in the social avoidance test (j), and the distance traveled in the
775 dark compartment in the light/dark transition test, in mice from the OF group. N = 6 for
776 each condition.

777

778 **Figure 4. Histone H1 lactylation in the brain is increased by social stress.** (a) Double
779 immunostaining of Kla and histone H1 in the mouse PFC. Arrows indicate Kla-negative and
780 histone H1-positive Hoechst-stained cells, and arrowheads indicate Kla-negative and
781 histone H1-negative Hoechst-stained cells. Scale bar: 50 μm. (b) Venn diagram showing the

bioRxiv preprint doi: https://doi.org/10.1101/2021.02.02.428370; this version posted February 4, 2021. The copyright holder for this preprint (which was not certified by peer review) is the author/funder, who has granted bioRxiv a license to display the preprint in perpetuity. It is made available under aCC-BY-NC-ND 4.0 International license.

782 overlap between Kla-positive and histone H1-positive cells in the mouse PFC. (c) Super-
783 resolution images of Kla and histone H1 in the nuclei of neurons of socially defeated mice
784 recorded with STED microscopy. Arrowheads indicate Kla- and histone H1-double–positive
785 structures. Scale bars: 5 µm (upper panels), 1 µm (lower panels). (d) Bar graphs show the
786 percentage of Kla and histone H1 merged area in the nucleus. N = 18 cells from 3 mice for
787 each condition. *P = 0.012, linear regression analysis.
788

bioRxiv preprint doi: https://doi.org/10.1101/2021.02.02.428370; this version posted February 4, 2021. The copyright holder for this preprint (which was not certified by peer review) is the author/funder, who has granted bioRxiv a license to display the preprint in perpetuity. It is made available under aCC-BY-NC-ND 4.0 International license.

789 Figure 1

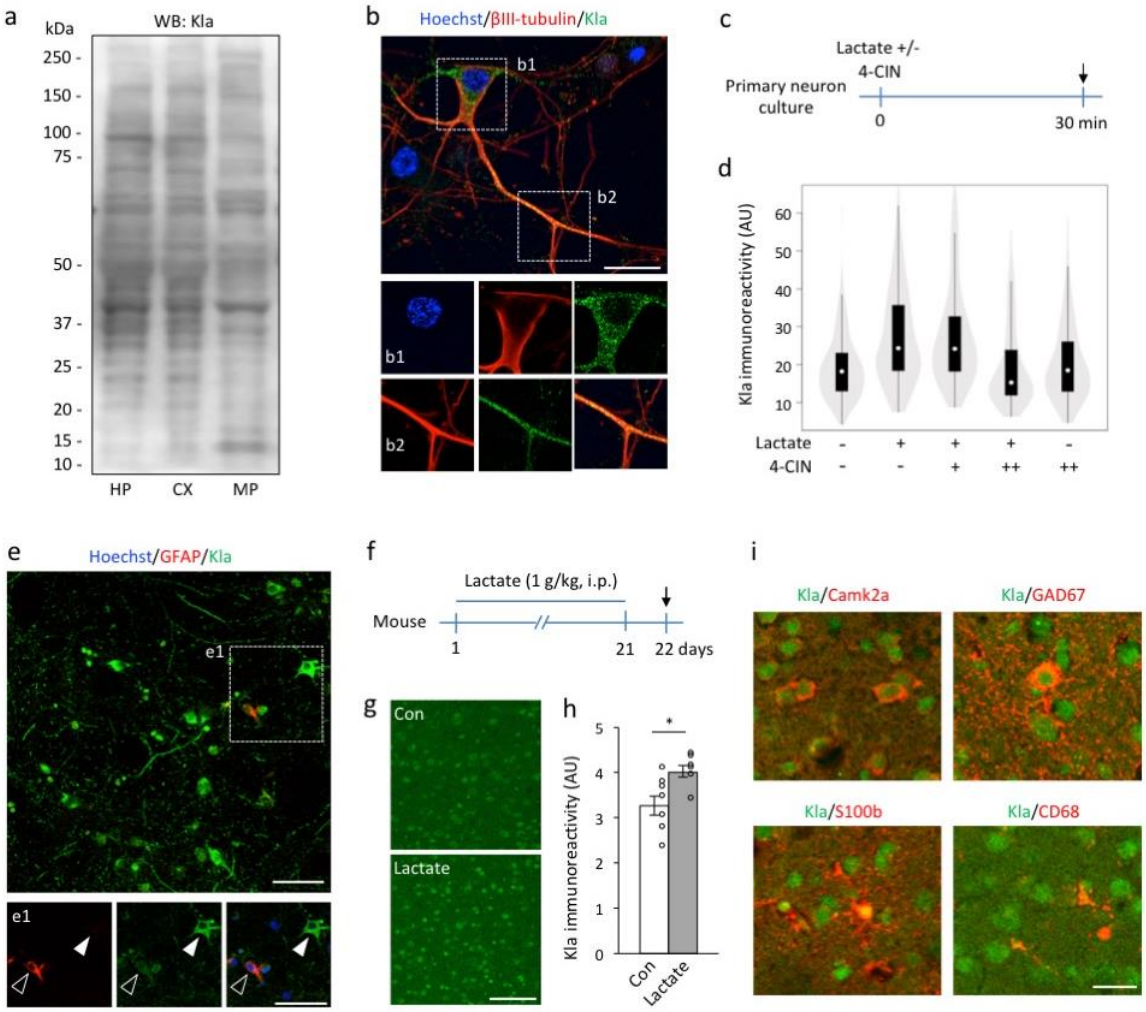

790

791

bioRxiv preprint doi: https://doi.org/10.1101/2021.02.02.428370; this version posted February 4, 2021. The copyright holder for this preprint (which was not certified by peer review) is the author/funder, who has granted bioRxiv a license to display the preprint in perpetuity. It is made available under aCC-BY-NC-ND 4.0 International license.

792 Figure 2

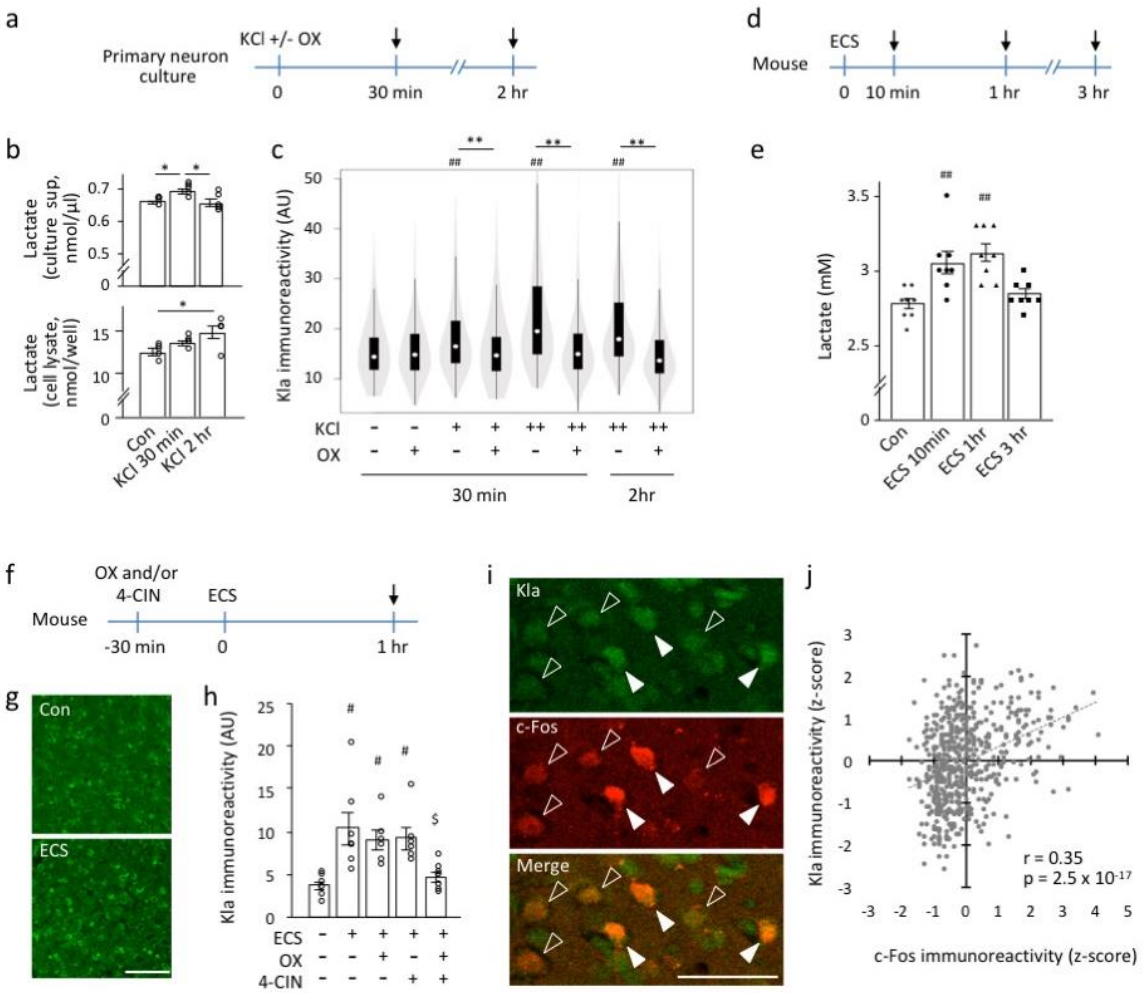

793

794

bioRxiv preprint doi: https://doi.org/10.1101/2021.02.02.428370; this version posted February 4, 2021. The copyright holder for this preprint (which was not certified by peer review) is the author/funder, who has granted bioRxiv a license to display the preprint in perpetuity. It is made available under aCC-BY-NC-ND 4.0 International license.

795 Figure 3

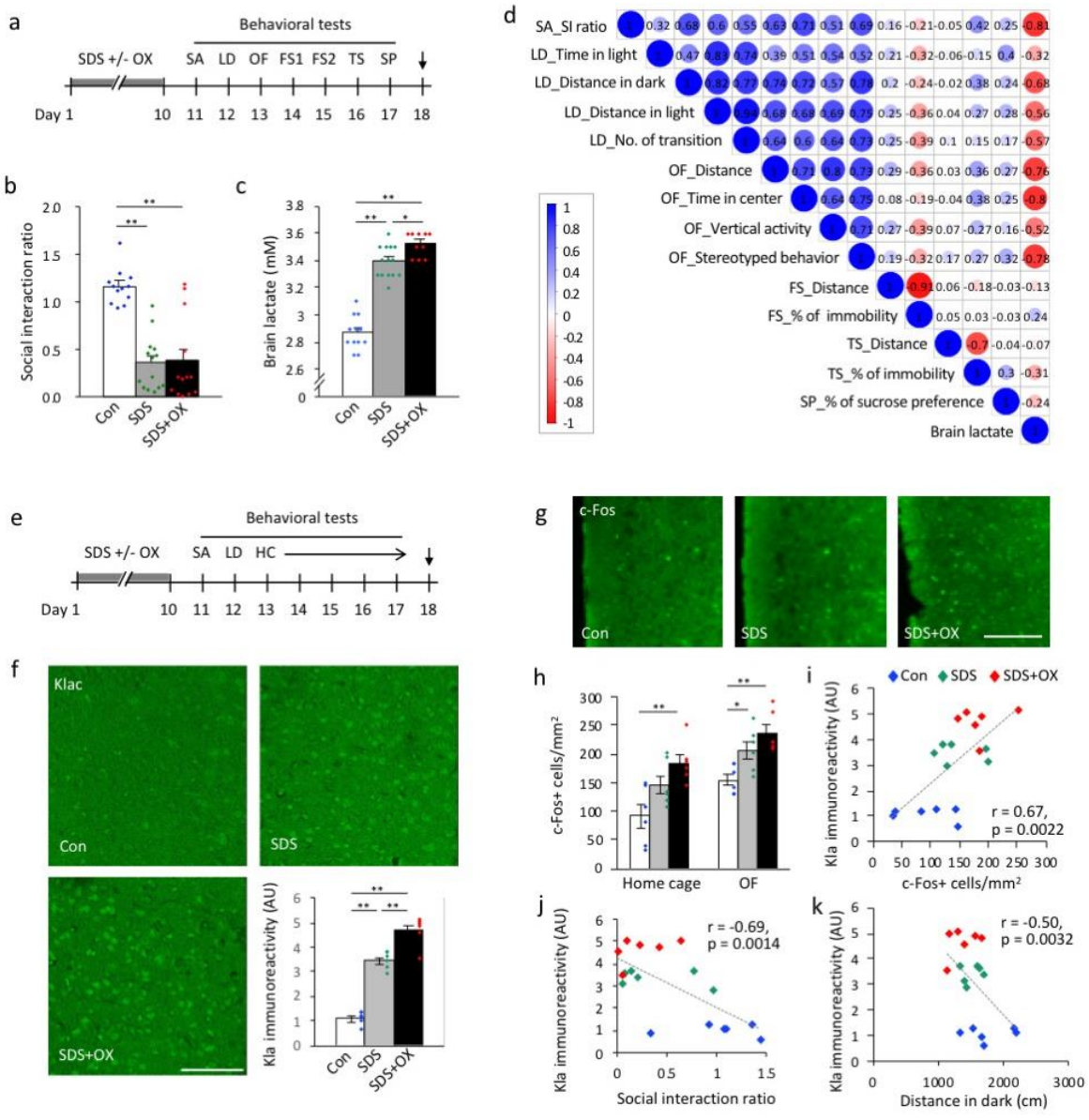

796

797

bioRxiv preprint doi: https://doi.org/10.1101/2021.02.02.428370; this version posted February 4, 2021. The copyright holder for this preprint (which was not certified by peer review) is the author/funder, who has granted bioRxiv a license to display the preprint in perpetuity. It is made available under aCC-BY-NC-ND 4.0 International license.

798 Figure 4

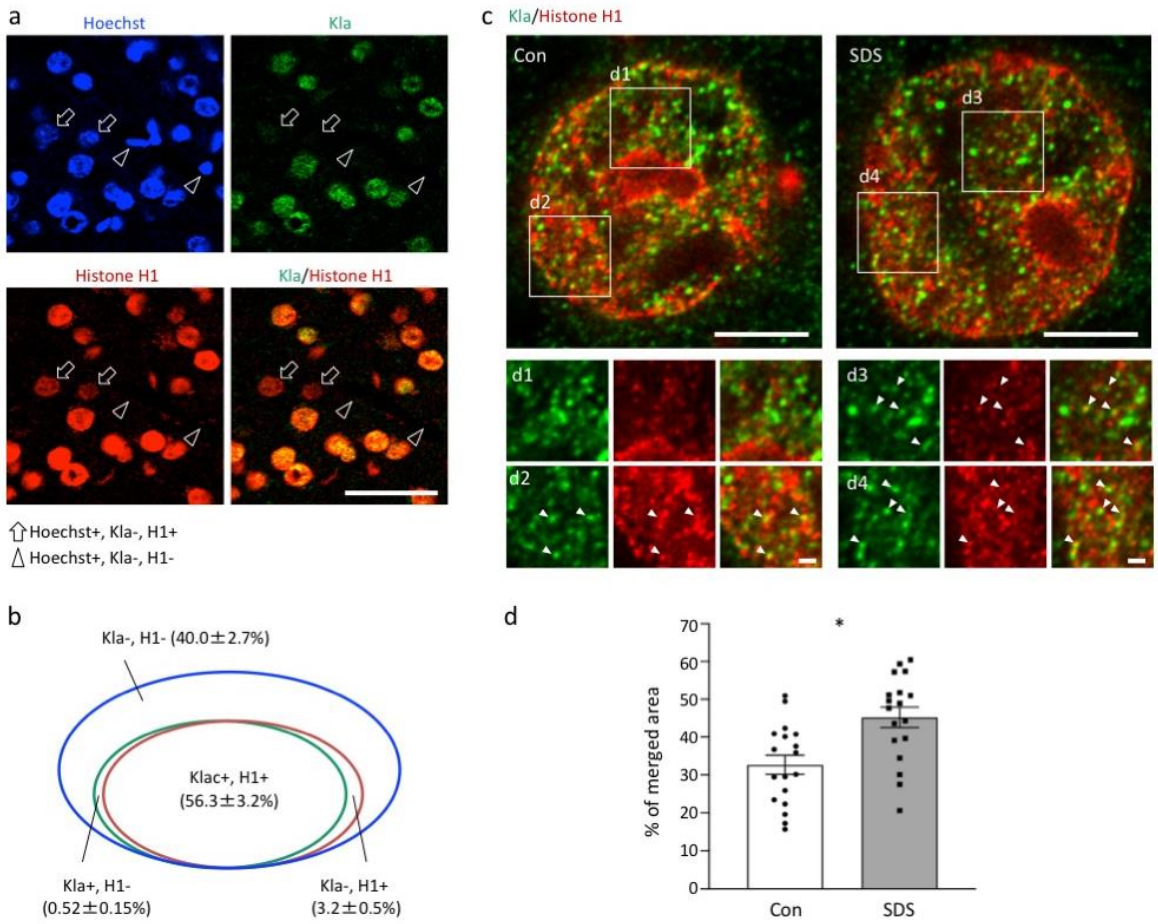

799

800